AD-A064 132 TETRA TECH INC PASADENA CALIF   F/G 20/4
             NONLINEAR THEORY FOR PARTIALLY CAVITATING CASCADE FLOWS.(U)
             SEP 78 O FURUYA   N00014-78-C-0146
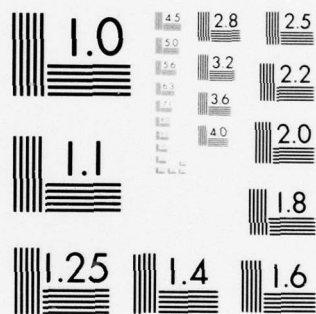UNCLASSIFIED   TETRAT-TC-3951-01   NL

| OF |
AD
A064132

END
DATE
FILMED
4—79
DDC

1.0

4.5
5.0
5.6
6.3

2.8

2.5

1.1

3.2

3.6

4.0

2.2

2.0

1.8

1.25 1.4 1.6

MICROCOPY RESOLUTION TEST CHART
NATIONAL BUREAU OF STANDARDS-1963-A

ADA064132

LEVEL II

(1)

TECH TECH

TETRA TECH

Report No. TC 3951-01
Contract No. N00014-78-C-0146

NONLINEAR THEORY FOR PARTIALLY
CAVITATING CASCADE FLOWS

By

OKITSUGU FURUYA

TETRA TECH, INC.
630 NORTH ROSEMEAD BOULEVARD
PASADENA, CALIFORNIA 91107

SEPTEMBER, 1978

D D C
RECEIVED
FEB 2 1979
RECEIVED
A

Prepared for
DAVID W. TAYLOR NAVAL SHIP R&D CENTER
BETHESDA, MARYLAND 20084

OFFICE OF NAVAL RESEARCH
800 NORTH QUINCY STREET
ARLINGTON, VIRGINIA 22217

79 01 31 005

Report No. TC 3951-01
Contract No. N00014-78-C-0146

NONLINEAR THEORY FOR PARTIALLY
CAVITATING CASCADE FLOWS

By

OKITSUGU FURUYA

TETRA TECH, INC.
630 NORTH ROSEMEAD BOULEVARD
PASADENA, CALIFORNIA 91107

SEPTEMBER, 1978

Prepared for
DAVID W. TAYLOR NAVAL SHIP R&D CENTER
BETHESDA, MARYLAND 20084

OFFICE OF NAVAL RESEARCH
800 NORTH QUINCY STREET
ARLINGTON, VIRGINIA 22217

Approved for public release;
distribution unlimited

79 01 31 005

REPORT DOCUMENTATION PAGE		READ INSTRUCTIONS BEFORE COMPLETING FORM
1. REPORT NUMBER TC 3951-01	2. GOVT ACCESSION NO.	3. RECIPIENT'S CATALOG NUMBER
4. TITLE (and Subtitle) Nonlinear Theory for Partially Cavitating Cascade Flows.		5. TYPE OF REPORT & PERIOD COVERED Technical-Theory February 15, 1978–Oct. 15, 1978
		6. PERFORMING ORG. REPORT NUMBER TC 3951-01
7. AUTHOR(s) Okitsugu Furuya		8. CONTRACT OR GRANT NUMBER(s) N00014-78-C-0146
9. PERFORMING ORGANIZATION NAME AND ADDRESS TETRA TECH, INC. 630 North Rosemead Boulevard Pasadena, California 91107		10. PROGRAM ELEMENT, PROJECT, TASK AREA & WORK UNIT NUMBERS DWTNSR&DC 8241967/9-1-77(1505)
11. CONTROLLING OFFICE NAME AND ADDRESS David W. Taylor Naval Ship R&D Center Department of the Navy Bethesda, Maryland 20084		12. REPORT DATE September 1978
		13. NUMBER OF PAGES 37
14. MONITORING AGENCY NAME & ADDRESS(if different from Controlling Office) Office of Naval Research 800 North Quincy Street Arlington, Virginia 22217		15. SECURITY CLASS. (of this report) Unclassified
		15a. DECLASSIFICATION/DOWNGRADING SCHEDULE

16. DISTRIBUTION STATEMENT (of this Report)

Approved for public release; distribution unlimited

TETRAT-TC-3951-01

17. DISTRIBUTION STATEMENT (of the abstract entered in Block 20, if different from Report)

Technical rept.
15 Feb – 15 Oct 78,

18. SUPPLEMENTARY NOTES

Sponsored by the Naval Sea Systems Command General Hydrodynamic Research Program and administered by the David W. Taylor Naval Ship R&D Center, Code 1505, Bethesda, Maryland 20084.

19. KEY WORDS (Continue on reverse side if necessary and identify by block number)

Partial cavity flow
Cascade
Nonlinear theory

20. ABSTRACT (Continue on reverse side if necessary and identify by block number)

A nonlinear theory for solving partially cavitating cascade problems was formulated in two different types of input data set-ups, one specifying cavitation number and the other the cavity length. The second method was necessary to find a unique solution because the cavity length has two different values for a specified cavitation number in some blade geometry cases. This fact, together with the investigation of detailed pressure distributions on the upper wetted part of the blade, explained the unsteady cavity phenomena previously reported in some experiments. Suggestions were made on how to avoid the occurrence of the unsteady partial cavity phenomena when one designs fluid machinery used in a partially cavitating regime.

DD FORM 1473 EDITION OF 1 NOV 65 IS OBSOLETE
1 JAN 73
S/N 0102-014-6601 |

TABLE OF CONTENTS

I.   SUMMARY

A nonlinear theory for solving partially cavitating cascade problems
was formulated in two different types of input data set-ups, one
specifying cavitation number and the other the cavity length. The
second method was necessary to find a unique solution because the
cavity length has two different values for a specified cavitation
number in some blade geometry cases. This fact, together with the
investigation of detailed pressure distributions on the upper wetted
part of the blade, explained the unsteady cavity phenomena previ-
ously reported in some experiments. Suggestions were made on how
to avoid the occurrence of the unsteady partial cavity phenomena
when one designs fluid machinery used in a partially cavitating
regime.

II.   ACKNOWLEDGMENTS

IV.   NOMENCLATURE

$\tilde{A}$ scale factor for mapping between W and ζ planes.

b ξ-coordinate corresponding to the upper cavity separation
         point

c ξ-coordinate corresponding to the cavity reattachment position
         and also used as a chord length of blade

C_L, C_D lift and drag coefficients parallel and normal to the
         incoming flow direction

$$\left(= L \text{ or } D / \tfrac{1}{2} \rho U_1^2 c \right)$$

$\overline{C}_L, \overline{C}_D$ lift and drag coefficients in the direction of the
         x and y axes

C_{Lm} lift coefficients in the x-direction normalized by
         the geometric mean velocity U_m

C_p pressure coefficient $\left(= \left(p - p_1 \right) / \tfrac{1}{2} \rho U_1^2 \right)$

D   drag force

d   spacing of cascade blades

f ξ-coordinate corresponding to the upper trailing edge

f_i nonlinear equations representing the boundary value
         problem for unknown solution parameters x_i

i   index for complex variable $\left(= \sqrt{-1} \right)$

L   lifting force

ℓ_c cavity length

p   static pressure

q   flow velocity modulus

S_1, S_2 total arc lengths of the upper and lower wetted part
         of the blade, respectively

$s(\xi)$ local arc length measured from either the leading edge or the reattachment point of cavity

sg(x)   sign function $\begin{pmatrix} = 1 \text{ for } x \geq 0 \\ =-1 \text{ for } x < 0 \end{pmatrix}$

TH   thickness of plano-convex blade normalized by chord

U   flow velocity amplitude

W   complex potential $= \left(\Phi + i\Psi\right)$

z   physical plane $\left(= x + iy\right)$

α flow angle made with the x-axis of the physical plane

β local blade slope measured from the x-axis, clockwise negative; for the second arc S_2, $-\pi$ is to be added

γ geometric stagger angle

δ stagger angle of the potential plane cascade set-up $\left(= \alpha_1 + \gamma\right)$

ζ transform potential plan $\left(= \xi + i\eta\right)$

ζ_1 ζ-coordinate corresponding to the upstream infinity of the physical plane

η vertical coordinate in the ξ-plane

θ flow angle

ξ horizontal coordinate in the ζ-plane

σ cavitation number $\left(= (p_1 - p_c)/\tfrac{1}{2}\rho U_1^2\right)$

τ logarithmic velocity normalized by U_2 $\left(= \ell n(q/U_2)\right)$

Φ potential function

Ψ stream function

ω hodograph variable $\left(= \theta + i\tau\right)$

Subscripts:

1 and 2   denotes quantities belonging to the upstream and
          downstream infinities, respectively, or
          quantities belonging to the first and second
          arcs, respectively

c   denotes the cavity

m   denotes geometric mean quantities

Superscripts:

+, -,   quantities belonging to the immediate upper and
          lower sides of the ξ-axis

1.   INTRODUCTION

It is a common practice that hydrodynamists avoid high speed
fluid machinery or components to be used under partially cavi-
tating conditions because many adverse hydrodynamic effects exist
for such conditions. One of the most important phenomena is that
of cavitation damage caused by cavity bubble collapse taking
place near the material. This material damage is so severe that
components such as marine propellers after several hundred hours
of exposure to cavity collapse will become totally out of use
(see e.g. [1]* for such examples). Furthermore, it was found
in experiments that partially cavitating flows experience inher-
ent unsteady flow phenomena; the length of cavity changes from
a very short one to one chord length in an oscillatory way (see
e.g. [2] and [3]). It is for this reason that effort by the
designer is directed toward either totally avoiding cavitating
conditions, if this is possible, or purposely generating super-
cavitating conditions in which cavity length is larger than the
body and thus bubble collapse occurs behind the material.

However, in recent years some marine and fluid machinery have
quite often been used in the partially cavitating flow regime.
One such example is in the marine propeller area; convential and
supercavitating propellers are sometimes used under off-design
conditions, the former at a lower advance speed and the latter

_____
* Numbers in brackets designate references at end of paper.

1

at a higher advance speed than that of the design point. In both cases some portions of propeller blades have partial cavities as were shown in experimental works by Sontvedt [4], Bohn [5] and Peck [6].

There exists more positive designers' attitude of using the partially cavitating condition in some area of fluid machinery such as pump inducers. Cavitating inducers used, for example, in liquid propellant rockets always operate at a partially cavitating condition. Because of simplicity, such inducer blades are made of helical profile having long straight-line face. The cavity length is designed to be always shorter than the chord length (see the work of Acosta [7]).

Interest has therefore grown recently in how to analytically determine the force coefficients of partially cavitating single foil or cascade blades. Linearized theories were applied by many researchers for both single and cascade blades. The former include works by Acosta [8], Geurst [9], Geurst and Verbrugh [10], Wade [11] and Golden [12]. Acosta [8] and Geurst [9] treated the flat plate single foil problem and Geurst and Verbrugh [10] solved the problem for camber line profiles. Wade [11] and Golden [12] considered both camber and thickness effects in the same linearized theory framework but with different solution methods; the former used an analytical solution method for vortex and source distributions whereas the latter employed a

numerical method to determine the strength of the singularities. For cascade configurations, Wade [13] solved flat plate cascade problems in exactly the same manner as for single foils. Algebra for the cascade flow becomes more complicated due to extra cascade mapping necessary for this case.

As has been seen above, all the existing analytical methods regarding the partially cavitating flow employed the linearized theories. The limitations of such theories are well described in each paper [8-13]; any perturbed flow quantities due to the existence of cavity and obstacle in the uniform flow should be small. Ranges of flow incidence angle, cavitation number and camber of blades for which the accuracy of the linearized theory is maintained to a desirable degree are not known until comparisons with experiments are made. Questions particularly arise for the linearization procedure for the nonlinear boundary condition on the cavity wall. Unlike the supercavitating flow regime, the cavitation number σ is relatively large compared to the uniform flow velocity. Nevertheless, all the linearized theories mentioned above assumed σ to be small. Furthermore, partially cavitating flow around the cascade having relatively high solidity will generate large disturbed velocity components for which the application of the linearized theory is no longer valid.

Under the circumstances just described, an analytical tool for determining the hydrodynamic forces of partially cavitating

cascade blades has been developed. The method used here is
the nonlinear potential theory, covering a complete range of geo-
metric configurations and flow parameters without generating any
inaccuracies in satisfying the boundary conditions. The method
is quite similar to that used for supercavitating cascade
flow analysis by Furuya [14], but with substantial increase in
complexity both in mathematical formulation and numerical com-
putations.

In the following sections, mathematical formulations and numer-
ical methods will be described. Some representative numerical
results will be compared with those of a linearized theory [13]
and an experiment [3].

2. NONLINEAR BOUNDARY VALUE PROBLEM

A mathematical model representing the physical flow of partial cavity around the cascade has to be established prior to the formulation of a nonlinear boundary value problem. The reattachment of cavity on the upper portion of the blade makes such a flow model construction difficult. Highly turbulent flows near the end point of cavity cannot be accurately represented within the framework of potential flow assumption currently taken. Among many possible flow models, we have chosen a most realistic one as shown in Figure 1. The cavity streamline detached from the leading edge of the blade terminates at point C, the location of which is either specified or determined as part of the solution as a function of cavitation number. This depends upon the type of input for boundary conditions, i.e., whether ℓ_c or σ is used as input data. Then the same streamline follows the body profile $\beta_2(x)$ through the trailing edge. The gap existing between the streamline and the upper body boundary is considered to be a turbulent wake region, which is implicitly eliminated from the present potential theory analysis. From the trailing edge, the wake with a constant pressure condition extends to the downstream infinity and is assumed to close there.

The end point of cavity is interesting from both physical and mathematical viewpoints. In the present flow model, the point C is termed as a single spiral vortex model named after Tulin

5

[16]. From the cavity side the streamline curls in to a point C, then immediately follows the corresponding body slope. It seems that this behavior of the streamline more or less represents the cavity collapse in the actual flow situation.

It must be noted that this type of cavity closure model may not be suitable for very thick foil cases, since the gap between the streamline and body boundary mentioned above is out of control. It may happen that the cavity ends inside the blade structure if the blade thickness is large. For such cases, one has to use an open wake cavity model in which the cavity closure condition at down infinity is relaxed but instead replaced by specifying the cavity thickness at the end point of cavity. In this way the streamline crossing problem mentioned above will be totally eliminated. The mathematical formulation for the open wake model is no more complicated than the closed wake. In this paper, however, the latter will be used throughout investigation.

The mathematical formulation is quite similar to that of the supercavitating cascade flow problem in [14], thus repetition of detailed explanations will be avoided.

The partially cavitating flow around the cascade shown in Figure 1 is first mapped onto the potential plane $W = \phi + i\Psi$ and then to the upper half of the transform plane ζ by the cascade mapping function, see Figures 2(a) and (b), respectively. The

cascade mapping function and its derivative are given by the following equations:

$$W = \frac{d}{2\pi} \left\{ e^{-i\delta} \ell n \, (1-\zeta/\zeta_1) + e^{i\delta} \ell n (1-\zeta/\bar{\zeta}_1) \right\} \tag{1}$$

where

$$\zeta_1 = \tilde{A} \, e^{i(\pi/2-\delta)} \tag{2}$$

$$\delta = \alpha_1 + \gamma, \tag{3}$$

and $\tilde{A}$ is a scaling factor between the two planes, yet to be known. Thus, the derivative of W on the ξ axis is given

$$\frac{dW}{d\xi} = \frac{d}{\pi} \frac{\xi \cos \delta}{(\xi - \tilde{A} \sin \delta)^2 + (\tilde{A} \cos \delta)^2}. \tag{4}$$

The stagger angle δ of the W-plane cascade set-up in Equation (3) was determined by the coordinate point (Φ_0, Ψ_0) where

$$\Phi_0 = dU_1 \cdot \sin (\alpha_1 + \gamma)$$
$$\Psi_0 = dU_1 \cdot \cos (\alpha_1 + \gamma). \tag{5}$$

Introducing a hodograph variable ω

$$\frac{dW}{dz} = q \, e^{-i\theta} = U_2 e^{-i\omega} \tag{6}$$

or

$$\omega = \theta + i \tau \tag{7}$$

$$\tau = \ell n (q/U_2) \tag{8}$$

where U_2 denotes the velocity at downstream infinity, we can express the boundary conditions on the real axis ξ in the ζ-plane as follows:

7

(i) $\tau = 0$, $-\infty < \xi < -1$, $f < \xi < \infty$

(ii) $\tau = \ell n \ (\sqrt{1 + \sigma}/U_2)$, $b < \xi < c$

(iii) $\theta = \begin{cases} \beta_1 \ (\equiv \tan^{-1} \ dy/dx) & -1 < \xi < 0 \\ \beta_1 + \pi & 0 < \xi < b \\ \beta_2 + \pi & c < \xi < f. \end{cases}$

This is a typical mixed-type boundary value problem, the solution of which can readily be found by the same approach as used in [14], but in a somewhat more complicated form due to the existence of two branch cuts, $-1 < \xi < b$ and $c < \xi < f$.

Analytically continuing the upper half of ξ-plane into the lower half plane with $\omega(\xi^*) = \omega^*(\xi)$, where * denotes the complex conjugate, these boundary conditions (i) - (iii) will be expressed as follows:

(i) $\omega^+ - \omega^- = 0$; $-\infty < \xi < -1$, $f < \xi < \infty$

(ii) $\omega^+ - \omega^- = 2i\ell n\left(\sqrt{1+\sigma}/U_2\right)$; $b < \xi < c$

(iii) $\omega^+ + \omega^- = 2\beta_1$; $-1 < \xi < 0$

                             $2(\beta_1 + \pi)$; $0 < \xi < b$

                             $2(\beta_2 + \pi)$; $c < \xi < f.$

The homogeneous part of the solution $H(\xi)$ for which the right hand sides of (i) - (iii) are all zero is obtained by considering the singularity at the end point of cavity and no singularities anywhere else;

8

$$H(\zeta) = \sqrt{\frac{(\zeta+1)(\zeta-b)(\zeta-f)}{\zeta-c}} \quad . \tag{9}$$

The general solution $G(\zeta)$ satisfying the mixed boundary conditions is defined by $G(\zeta) = \omega(\zeta)/H(\zeta)$ and obtained by applying the Cauchy integral formula;

$$G(\zeta) = \frac{1}{2\pi i} \int (G^+ - G^-) \frac{d\xi'}{\xi - \zeta} \, .$$

Therefore,

$$\omega(\zeta) = H(\zeta)G(\zeta)$$

$$= \sqrt{\frac{(\zeta+1)(\zeta-b)(\zeta-f)}{\zeta-c}} \ \frac{1}{2\pi i} \left\{ \int_{-1}^{b} \frac{2\beta_1}{i\sqrt{\frac{(\xi'+1)(b-\xi')(\xi'-f)}{\xi'-c}}} \ \frac{d\xi'}{\xi'-\zeta} \right.$$

$$+ \int_{0}^{b} \frac{2\pi}{i\sqrt{\frac{(\xi'+1)(b-\xi')(\xi'-f)}{\xi'-c}}} \ \frac{d\xi'}{\xi'-\zeta} + \int_{b}^{c} \frac{2i \, \ln\left(\sqrt{1+\sigma}/U_2\right)}{\sqrt{\frac{(\xi'+1)(\xi'-b)(\xi'-f)}{\xi'-c}}} \ \frac{d\xi'}{\xi'-\zeta}$$

$$\left. + \int_{c}^{f} \frac{2\beta_2 + 2\pi}{i\sqrt{\frac{(\xi'+1)(\xi'-b)(f-\xi')}{\xi'-c}}} \ \frac{d\xi'}{\xi'-\zeta} \right\} \, . \tag{10}$$

2.1 BOUNDARY VALUE PROBLEM   TYPE I (SPECIFY CAVITATION NUMBER σ)

For the problem in which the cavitation number is specified as an input parameter, the length of cavity is to be determined as part of the solution. In such a problem we have a total of six unknown quantities, U_2, α_2, $\tilde{A}$, b, c, f, requiring six equations to determine them uniquely;

9

(i)   At the upstream infinity,

$\omega(\zeta_1) = \alpha_1 + i \ln(1/U_2)$:   2 equations

(ii)   At the downstream infinity,

$\omega(\infty) = \alpha_2$:   1 equation

(iii)   Length of First Arc $\equiv S_1$:   1 equation

(iv)   End point of the streamline
           ($\xi=f$) matches the physical
           trailing edge: 1 equation

(v)   Continuity Equation: 1 equation

where S_1 and S_2 are depicted in Figure 2(c). It is noted that the arc length condition (iv) replaces the potential difference condition in the supercavitating cascade problem. (see Reference [14])

Application of these conditions to Equation (10) yields the following six equations;

i)   **At Upstream Infinity:**

$$\begin{Bmatrix} f_1 \\ f_2 \end{Bmatrix} \equiv \sqrt{\frac{(\zeta_1+1)(\zeta_1-b)(\zeta_1-f)}{\zeta_1-c}} \Bigg\rbrace - \frac{1}{\pi} \int_{-1}^{b} \frac{\beta_1}{\sqrt{\frac{(\xi'+1)(b-\xi')(\xi'-f)}{\xi'-c}}} \frac{d\xi'}{\xi'-\zeta_1}$$

$$- \int_{0}^{b} \frac{1}{\sqrt{\frac{(\xi'+1)(b-\xi')(\xi'-f)}{\xi'-c}}} \frac{d\xi'}{\xi'-\zeta_1} + \frac{1}{\pi} \ln\left(\frac{\sqrt{1}+\sigma}{U_2}\right) x$$

$$\int_{b}^{c} \frac{1}{\sqrt{\frac{(\xi'+1)(\xi'-b)(\xi'-f)}{\xi'-c}}} \frac{d\xi'}{\xi'-\zeta_1} - \frac{1}{\pi} \int_{c}^{f} \frac{\beta_2+\pi}{\sqrt{\frac{(\xi'+1)(\xi'-b)(f-\xi')}{\xi'-c}}} \frac{d\xi'}{\xi'-\zeta_1} \Bigg\rbrace$$

$$- \left\{ \alpha_1 + i \ln(1/U_2) \right\} = 0 \qquad (11)$$

10

ii)   <u>At Downstream Infinity:</u>

$$f_3 \equiv \frac{1}{\pi} \int_{-1}^{b} \frac{\beta_1}{\sqrt{\dfrac{(\xi'+1)(b-\xi')(\xi'-f)}{\xi'-c}}} \, d\xi' + \int_{0}^{b} \frac{d\xi'}{\sqrt{\dfrac{(\xi'+1)(b-\xi')(\xi'-f)}{\xi'-c}}}$$

$$- \frac{1}{\pi} \ell n \left(\frac{\sqrt{1+\sigma}}{U_2} \right) \int_{b}^{c} \frac{d\xi'}{\sqrt{\dfrac{(\xi'+1)(\xi'-b)(\xi'-f)}{\xi'-c}}} +$$

$$\frac{1}{\pi} \int_{c}^{f} \frac{\beta_2 + \pi}{\sqrt{\dfrac{(\xi'+1)(\xi'-b)(f-\xi)}{\xi'-c}}} \, d\xi' - \alpha_2 = 0 \qquad (12)$$

iii)   First Arc Length = S_1:

On the wetted part of the streamline,

$$\frac{dz}{ds_1} = e^{i\beta_1}$$

thus

$$ds_1 = e^{-i\beta} \frac{e^{i\omega}}{U_2} \frac{dW}{d\xi} \, d\xi \; .$$

For $-1 < \xi < b$, $\omega(\zeta)$ can be written as follows;

$$\omega(\xi) = \begin{cases} ig_1(\xi) + \beta_1(\xi) & , \quad -1 < \xi < 0 \\ ig_1(\xi) + \beta_1(\xi) + \pi, & \quad 0 < \xi < b \end{cases}$$

11

where

$$g_1(\xi) = \left. \sqrt{\frac{(\xi+1)(b-\xi)(\xi-f)}{\xi-c}} \right\} - \frac{1}{\pi} \oint_{-1}^{b} \frac{\beta_1}{\sqrt{\frac{(\xi'+1)(b-\xi')(\xi'-f)}{\xi'-c}}} \frac{d\xi'}{\xi'-\xi}$$

$$-\oint_{0}^{b} \frac{1}{\sqrt{\frac{(\xi'+1)(b-\xi')(\xi'-f)}{\xi'-c}}} \frac{d\xi'}{\xi'-\xi} + \frac{1}{\pi} \ln\left(\frac{\sqrt{1+\sigma}}{U_2}\right) x$$

$$\left. \int_{b}^{c} \frac{1}{\sqrt{\frac{(\xi'+1)(\xi'-b)(\xi'-f)}{\xi'-c}}} \frac{d\xi'}{\xi'-\xi} - \frac{1}{\pi} \int_{c}^{f} \frac{\beta_2+\pi}{\sqrt{\frac{(\xi'+1)(\xi'-b)(f-\xi')}{\xi'-c}}} \frac{d\xi'}{\xi'-\xi} \right\} . \quad (13)$$

After integrating the above equation, one finds;

$$s_1(\xi) = \int_{\xi}^{b} sg(\xi) \frac{e^{-g_1(\xi)}}{U_2} \frac{dW}{d\xi} d\xi$$

where

$$sg(\xi) = \begin{cases} 1 & , & \xi > 0 \\ -1 & , & \xi < 0. \end{cases}$$

The arc length condition is therefore satisfied by the follow-
ing equation;

$$f_4 \equiv S_1 - s_1(-1) = 0 \qquad (14)$$

where $dW/d\xi$ is given by Equation (4).

iv) <u>End Point of the Streamline at $\xi = f$ Matching the Trailing Edge
of the Blade</u>:

Similar to the above derivation, the equation f_5 is obtained as
follows:

12

$$f_5 \equiv S_2 - s_2 \, (f) = 0 \tag{15}$$

where
$$s_2(\xi) = \int_c^\xi \frac{e^{-g_2(\xi)}}{U_2} \; \frac{dW}{d\xi'} \, d\xi'$$

and
$$g_2(\xi) = \sqrt{\frac{(\xi+1)(\xi-b)(f-\xi)}{\xi-c}} \left\{ - \frac{1}{\pi} \int_{-1}^b \frac{\beta_1}{\sqrt{\frac{(\xi'+1)(b-\xi')(\xi'-f)}{\xi'-c}}} \; \frac{d\xi'}{\xi'-\xi} \right.$$

$$- \int_0^b \frac{1}{\sqrt{\frac{(\xi'+1)(b-\xi')(\xi'-f)}{\xi'-c}}} \; \frac{d\xi'}{\xi'-\xi} + \frac{1}{\pi} \, \ell n \left(\frac{\sqrt{1+\sigma}}{U_2} \right) x$$

$$\int_b^c \frac{1}{\sqrt{\frac{(\xi'+1)(\xi'-b)(\xi'-f)}{\xi'-c}}} \; \frac{d\xi'}{\xi'-\xi} - \frac{1}{\pi} \oint_c^f \frac{\beta_2+\pi}{\sqrt{\frac{(\xi'+1)(\xi'-b)(f-\xi')}{\xi'-c}}} \; \frac{d\xi'}{\xi'-\xi} \left. \right\} \cdot (16)$$

In order to determine the second arc length S_2, the end point of cavity should be known. The cavity shape is expressed in terms of ξ-coordinate;

$$x-x_B = \frac{1}{\sqrt{1+\sigma}} \int_b^\xi \cos g_c(\xi') \; \frac{dW}{d\xi'} \, d\xi' \tag{17}$$

$$y-y_B = \frac{1}{\sqrt{1+\sigma}} \int_b^\xi \sin g_c(\xi') \; \frac{dW}{d\xi'} \, d\xi' \tag{18}$$

13

where

$$g_c(\xi) \sqrt{\frac{(\xi+1)\ (\xi-b)\ (f-\xi)}{c-\xi}} \Bigg\} - \frac{1}{\pi} \int_{-1}^{b} \frac{\beta_1(\xi')}{\sqrt{\frac{(\xi'+1)(b-\xi')(\xi'-f)}{\xi'-c}}} \frac{d\xi'}{\xi'-\xi}$$

$$-\int_{0}^{b} \frac{1}{\sqrt{\frac{(\xi'+1)(b-\xi')(\xi'-f)}{\xi'-c}}} \frac{d\xi'}{\xi'-\xi} + \frac{1}{\pi} \ln\left(\frac{\sqrt{1+\sigma}}{U_2}\right) X$$

$$\oint_{b}^{c} \frac{1}{\sqrt{\frac{(\xi'+1)(\xi'-b)(\xi'-f)}{\xi'-c}}} \frac{d\xi'}{\xi'-\xi} - \frac{1}{\pi} \int_{c}^{f} \frac{\beta_2+\pi}{\sqrt{\frac{(\xi'+1)(\xi'-b)(f-\xi')}{\xi'-c}}} \frac{d\xi'}{\xi'-\xi} \Bigg\} \cdot \quad (19)$$

x_B, y_B are the physical coordinates of the blade leading edge.
The end point of the cavity $(x_c,\ y_c)$ is obtained by setting the
upper bound of the above integrals (17) and (18) to be c. Once
$(x_c,\ y_c)$ are determined, the second arc length S_2 is easily
calculated by following the body profile.

v) Continuity Equation:

The mass flow condition for the upstream and downstream is given
as;

$$f_6 \equiv U_1 \cos(\alpha_1+\gamma) \cdot d - U_2 \cos(\alpha_2+\gamma) \cdot d = 0 \qquad (20)$$

Equations (11), (12), (14), (15) and (20) now provide six
independent relationships for six unknown parameters.

14

2.2 BOUNDARY VALUE PROBLEM TYPE II (SPECIFY CAVITY LENGTH ℓ_c)

The cavity length ℓ_c is used as   input data in this case and
the corresponding cavitation number σ is determined as a result
of the solution. Minor changes to the TYPE I problem are neces-
sary. In addition to f_5 in Equation (15), one more equation,
f_7, is added in order to satisfy the fixed cavity length con-
dition.

$$f_7 \equiv x_c - \ell_c = 0 \tag{21}$$

where x_c is calculated by setting ξ to be c in Equation (17).
We have now seven independent equations for seven unknown solu-
tion parameters including σ.

There is absolutely no difference in final solutions between
the above two boundary value problems as long as the physical
and geometric flow conditions are the same. In many actual cases,
the cavitation number, which can be simply determined by the
upstream static pressure and vapor pressure, is a specified in-
put rather than the cavity length. Only the first type of
B.V.P. is therefore usually used to provide solutions
for the problem like supercavitating flows. Special reasons
for introducing the second type of B.V.P. in this study exist:

    i)   Increase the stability of the numerical iterative
        method by fixing the wetted portion of the upper
        blade, and

    ii)   Avoid the numerical instability caused by the existence
        of multiple cavity-length solutions for one cavita-
        tion number as reported in [9], [13] and [15].

15

As will be discussed in the following section, the numerical instability actually occurred for certain cases when the first type of B.V.P. was used, whereas cavitation number was uniquely determined for any specified cavity length when the second method was employed.

3.   NUMERICAL METHOD

The same Newton's functional iterative method as that in [14]
was applied to the present system of nonlinear functional
equations for determining the solution parameters. Representing
these equations and unknown parameters as

$$\underline{f}\ (\underline{x}) = 0, \tag{22}$$

the iterative method is introduced in the following relation;

$$J\left(\underline{x}^{\ (n)}\right) \cdot \left(\underline{x}^{(n+1)} - \underline{x}^{(n)}\right) = -f\left(\underline{x}^{(n)}\right) \tag{23}$$

where J is a partial derivative matrix whose component is
expressed

$$J \equiv \frac{\partial f_i}{\partial x_i}\ . \tag{24}$$

By assuming a starting set of $\underline{x}^{(n)}$ values, $\underline{x}^{(n+1)}$ will be
calculated based on Equation (23). As has been seen in the preceding
section, $\underline{f}$ also requires the information regarding β_1 and β_2 as
a function of ξ. Although the body inclinations β_1 and β_2 are
specified in the physical plane, we do not know them as a function
of mapped potential coordinate ξ until the complete problem is
solved. This inherently nonlinear implicit problem is conveniently
resolved as a part of the above iterative method by gradually
updating β_1 and β_2. The first assumption for β_1 and β_2 is naturally
that of constant values, i.e., straight line body assumption.
These values are then updated whenever the new set of $\underline{x}$ values are
obtained. The iteration procedure will be continued until $\underline{x}$ as well
as the functional relations for β_1 and β_2 against ξ converge.

17

4. PRESSURE DISTRIBUTIONS, FORCE COEFFICIENTS

Once a convergent solution is obtained, the calculations for C_p, C_L and C_D are straightforward.

Since

$$C_p = 1 - \left(q/U_1 \right)^2$$

and

$$q^2 = U_2^2 e^{-i(\omega - \omega^*)},$$

thus

$$C_p = 1 - U_2^2 \left[\exp \quad I_m \left\{ \omega(\xi) \right\} \right]^2 \tag{24}$$

where

$$I_m \left\{ \omega(\xi) \right\} = \begin{cases} g_1(\xi) & \text{for } -1 < \xi < b \\\\ \ln \sqrt{\dfrac{1+\sigma}{U_2}} & \text{for } b < \xi < c \\\\ g_2(\xi) & \text{for } c < \xi < f. \end{cases}$$

The functions $g_1(\xi)$ and $g_2(\xi)$ were already introduced in Equations (14) and (15).

The lift and drag coefficients in the direction of the x- and y- axes are given

$$\overline{C_L} = -\int_{-1}^{f} C_p \; \frac{dx}{ds} \cdot \frac{ds}{d\xi} \cdot d\xi \tag{25}$$

$$\overline{C_D} = \int_{-1}^{f} C_p \; \frac{dy}{ds} \cdot \frac{ds}{d\xi} \cdot d\xi \tag{26}$$

18

where

$$\frac{dx}{ds} = \begin{cases} \dfrac{dx}{ds_1} = \cos \beta_1 & \text{for the first arc } S_1 \\[4pt] & (-1<\xi<b) \\[10pt] \dfrac{dx}{ds_2} = -\cos \beta_2 & \text{for the second arc } S_2 \\[4pt] & (c<\xi<f) \end{cases}$$

$$\frac{dy}{ds} = \begin{cases} \sin \beta_1 & \text{for the first arc } S_1 \\[4pt] & (-1<\xi<b) \\[10pt] \sin \beta_2 & \text{for the second arc } S_2 \\[4pt] & (c<\xi<f) \end{cases}$$

$$\frac{ds}{d\xi} = \begin{cases} \dfrac{ds_1}{d\xi} = - sg\ (\xi)\ \dfrac{e^{-g_1(\xi)}}{U_2}\ \dfrac{dw}{d\xi} & \begin{array}{l} \text{for the} \\ \text{first arc } S_1 \\ (-1<\xi<b) \end{array} \\[16pt] \dfrac{ds_2}{d\xi} = \dfrac{e^{-g_2(\xi)}}{U_2}\ \dfrac{dW}{d\xi} & \begin{array}{l} \text{for the} \\ \text{second arc } S_2 \\ (c<\xi<f) \end{array} \end{cases}$$

The lift and drag coefficients C_L and C_D in parallel and normal to
the incoming flow angle are thus calculated

$$C_L = \overline{C_L} \cos \alpha_1 - \overline{C_D} \sin \alpha_1 \tag{27}$$

$$C_D = \overline{C_L} \sin \alpha_1 + \overline{C_D} \cos \alpha_1. \tag{28}$$

19

5.   RESULTS AND CONCLUSIONS

The present theory was first applied to partially cavitating
flat-plate cascades and the results were compared with those of
a linearized theory of Wade [13] where the same parameters in
[13] are used in Figure 3. Not only the lifting force itself
but also the trend of the curves are significantly different
between the two theories. The discrepancies particularly become
larger as the cavitation number increases. As has been mentioned
before, it is considered that these discrepancies are attributable
to the loss of the linearized theory's accuracy for larger cavi-
tation number flows. Furthermore, the incidence angle taken in
the nonlinear theory, i.e., 8 degrees, may be already beyond
the applicable range of the linearized theory.

The theory was also compared with some experimental data of par-
tially cavitating cascade of plano-convex blades [3]. The blade
thickness used for the experiment was 8 percent chord. In order
to gradually update the present numerical calculations, the
thickness of plano-convex blade was changed, starting from 0
percent to 2, 5 and 8 percents. Each computation utilized con-
verged solution of previous results as a starting point of the
iterative procedure. The lift and drag coefficients are shown
in Figures 4 and 5. Convergent solutions were obtained for 0
and 2 percent thickness cases with the TYPE I B.V.P. in which
the cavitation number was specified. The results not only
check with the lift coefficients of fully wetted flat plate

20

cascade calculated based on Thwaites [17], but also show the effects of blade camber as an increase in C_L. The calculated results of 2 percent thickness approach closer to those of the experiment having blades of 8 percent thickness.

We encountered severe numerical instability with the same computer program when the blade thickness was increased to 5 and 8 percents. No matter how carefully initial values were chosen, the length of cavity at each iteration wildly changed over a total range of chord length and never converged. It was this time that the TYPE II B.V.P. approach in which the cavity length is specified and the corresponding cavitation number is determined was used. The problem of numerical instability was resolved with this second method. As was suspected from the occurrence of numerical instability for thickness of 5 percents with the first method, it was found here that the cavity has two different lengths for one cavitation number as shown in Figure 6. The lift and drag coefficients obtained are also plotted in Figures 4 and 5 and showed peculiar behavior in the $C_L - \sigma$ and $C_D - \sigma$ curves. As the cavity length decreases, the cavitation number first increases but then starts decreasing with a slight increase of C_L. It seems that these multiple cavity length solutions and peculiar force-vs.-σ behaviors will well explain the unsteady oscillatory phenomena of the partially cavitating single foil or cascade flows as were observed in experiments [2] and [3]. A recent study of Uhlman and Jiang [15] attributed the existence of two cavity lengths for a specified σ to the inaccuracy of the linearized theory and the inherent flow instability. The first cause is now obviously denied.

21

The plano-convex foils such as of 0 and 2 percent thickness
have a single value of cavity length for a specified σ while as
the thickness increases to e.g., 5 percents the cavity length
starts having double values. This fact seems to provide an
essential key for understanding the above unsteady cavity phenomena.
The detailed pressure distributions on the upper blade surface
are plotted in Figures 7(a) to (c). For the thickness of 0 and
2 percent cases, it is seen from these figures that the pressure
distributions on the upper solid boundary always indicate positive
values relative to the cavity pressures C_{pc}. On the other hand,
for the blade thickness of 5 percent (Figure 7 (c)), these pressures
rapidly become negative relative to C_{pc}, particularly as the cavity
length becomes shorter. This violates a theorem applied to the
present boundary value problem that the minimum pressure exists
inside the cavity (see e.g., a textbook by Birkhoff and Zarantonello
[18]) . Furthermore, even taking viscous effects into consideration,
high negative pressures cannot be sustained in actual flow field,
indicating that the cavity is ready to extend to these lower
pressure regions. As soon as the cavity becomes longer, no more
low pressure field exists. As is seen in Figure 7 (c), e.g.,
$\sigma = .37$ case, the vaporization process is not fast enough to pro-
vide vapor to hold the cavity. The cavity bubble is thus shed
downstream and a new short cavity starts growing.

The generation of higher negative pressures for thicker blades
is easily understood; the higher the negative curvature of the
obstacle in the flow field, the lower the negative pressure.
As a matter of fact, the present explanation for the unsteady
partial cavity flow motion based on the steady state flow analysis

22

is consistent with experimental observations. Experiments of
Meijer [2] and Wade and Acosta [3] are two well-known cases in
which the unsteady phenomena were observed. Although one tested a
single foil and the others cascade foils, a most significant coin-
cidence between the two is that both used blades whose upper profile
is of unfavorable shape for the pressure field, i.e., concave shape,
in these cases, circular arc. It is now clearly explainable why
the unsteady cavity oscillations occurred in both cases.

Based on the above discussions, it is realized that the partially
cavitating flow is either stable or unstable, depending upon the
pressure distributions on the wetted part of the upper blade sur-
face. Figure 6 indicates the stable partial cavity condition
for thin flat-plate cascades. In the past, little hydrodynamic
considerations have been given for design of blade backside pro-
file. For example, the backside profiles of supercavitating
propellers were determined from a structural integrity point of
view within the limit of cavity envelope. In order to avoid the
occurrence of cavity oscillations if such propellers operate at
an off-design point in the partially cavitating regime, it is
recommended that the blade backside profile be properly designed
so that favorable pressure distributions Cp prevail. At least,
Cp on the backside of blades under several partially cavitating
conditions must be investigated during the design procedure; it
should be ensured that C_p is much larger than $-\sigma$ over the full
range of wetted upper boundary.

Unlike linearized partial cavity or super cavitating theories, the present nonlinear partial cavity theory has no singular behaviors as ℓ_c approaches the chord length nor does the nonlinear super-cavity theory [14]. In Figures 4 and 5, the regimes as ℓ_c becomes c are depicted by dashed lines. This does not mean that C_L and C_D are unknown or become infinite, but they simply have slight discrepancies between the two nonlinear theories because the flow models used for the partial and super-cavity regions cannot be smoothly blended.

Figure 8 shows the boundary profiles of typical partial cavities for $\alpha_1 = 9°$, $\gamma = 36°$ and blade thickness of 2 percents at various cavitation numbers or cavity lengths.

Finally, it must be noted that the numerical iterative method used here provided stable convergent solutions as long as one chose a right type of input data set-up as has been mentioned above. Computer execution time, however, was found to be two to six times that of supercavitating cascade computations in [14].

24

6.   REFERENCES

[1] Knapp, Daily and Hammit, CAVITATION, McGraw Hill Book
     Company, New York, 1970.

[2] Meijer, M.C., "Some Experiments on Partly Cavitating Hydro-
     foils", International Shipbuilding Progress, Vol. 6, No. 60,
     August 1959.

[3] Wade, R.B., and Acosta, A.J.,"Investigation of Cavitating
     Cascade", ASME, Journal of Basic Engineering, December 1967,
     693-706.

[4] Søndvedt, T. and Frivold, H., "Low Frequency Variation of
     the Surface Shape of Tip Region Cavitation on Marine Pro-
     peller Blades and Corresponding Disturbances on Nearby Solid
     Boundaries", Eleventh Symposium of Naval Hydrodynamics,
     Sponsored by the Office of Naval Research, University
     College London, 28 March-2 April 1976.

[5] Bohn, J.C., "Model Tests of a Supercavitating Propeller
     Designed for a Hydrofoil Ship", Hydronautics Technical Report,
     7607.59, August 1977.

[6] Peck, J.G., "Cavitation Performance Characteristics of
     Supercavitating Propellers 4698 and 4699", David W. Taylor
     Naval Ship Research and Development Center of the U.S.
     Navy, Ship Performance Department Report SPD-680-02,
     December 1977.

[7] Acosta, A.J., "An Experimental Study of Cavitating Inducers",
Second Symposium on Naval Hydrodynamics of Office of Naval
Research, August 25-29, 1958, Washington, D.C., 533-557.

[8] Acosta, A.J., "A Note on Partial Cavitation of Flat Plate
Hydrofoils", Hydrodynamics Lab., California Institute of
Technology, Report No. E-19.9, 1955.

[9] Geurst, J.A., "Linearized Theory for Partially Cavitated
Hydrofoils", International Shipbuilding Progress, Vol. 6,
No. 60, August 1959.

[10] Geurst, J.A., and Verbrugh, P.J.,"A Note on Camber Effects
of a Partially Cavitated Hydrofoil", International Ship-
building Progress, Vol. 6, No. 61, September 1959.

[11] Wade, R.B., "Linearized Theory of a Partially Cavitating
Plano-Convex Hydrofoil Including the Effects of Camber and
Thickness", Journal of Ship Research, Vol. 11, No. 1,
March 1967.

[12] Golden, D.W., "A Numerical Method for Two-Dimensional,
Cavitating, Lifting Flow", Report No. 81512-1, Department
of Ocean Engineering, M.I.T., May 1975.

[13] Wade, R.B., "Flow Past a Partially Cavitating Cascade of Flat Plate Hydrofoils", Division of Engineering and Applied Science, California Institute of Technology, Report No. E79-4, January 1963.

[14] Furuya, O., "Exact Supercavitating Cascade Theory", ASME, Journal of Fluids Engineering, Vol. 97, December 1975, 419-429.

[15] Uhlman, J.S., Jr., and Jiang, C.W., "Experiments on a Partially Cavitating Plano-Convex Hydrofoil with Comparison to Theory", M.I.T. Report No. 83481-2, July 1977.

[16] Tulin, M.P., "Supercavitating Flows -- Small Perturbation Theory", Journal of Ship Research, Vol. 13, No. 3, 1964, 16-37.

[17] Thwaites, B., INCOMPRESSIBLE AERODYNAMICS, Oxford at the Clarendon Press, 1960, 532.

[18] Birkhoff, G. and E.M. Zarantonello, JETS, WAKES, AND CAVITIES, Academic Press, Inc., New York 1957.
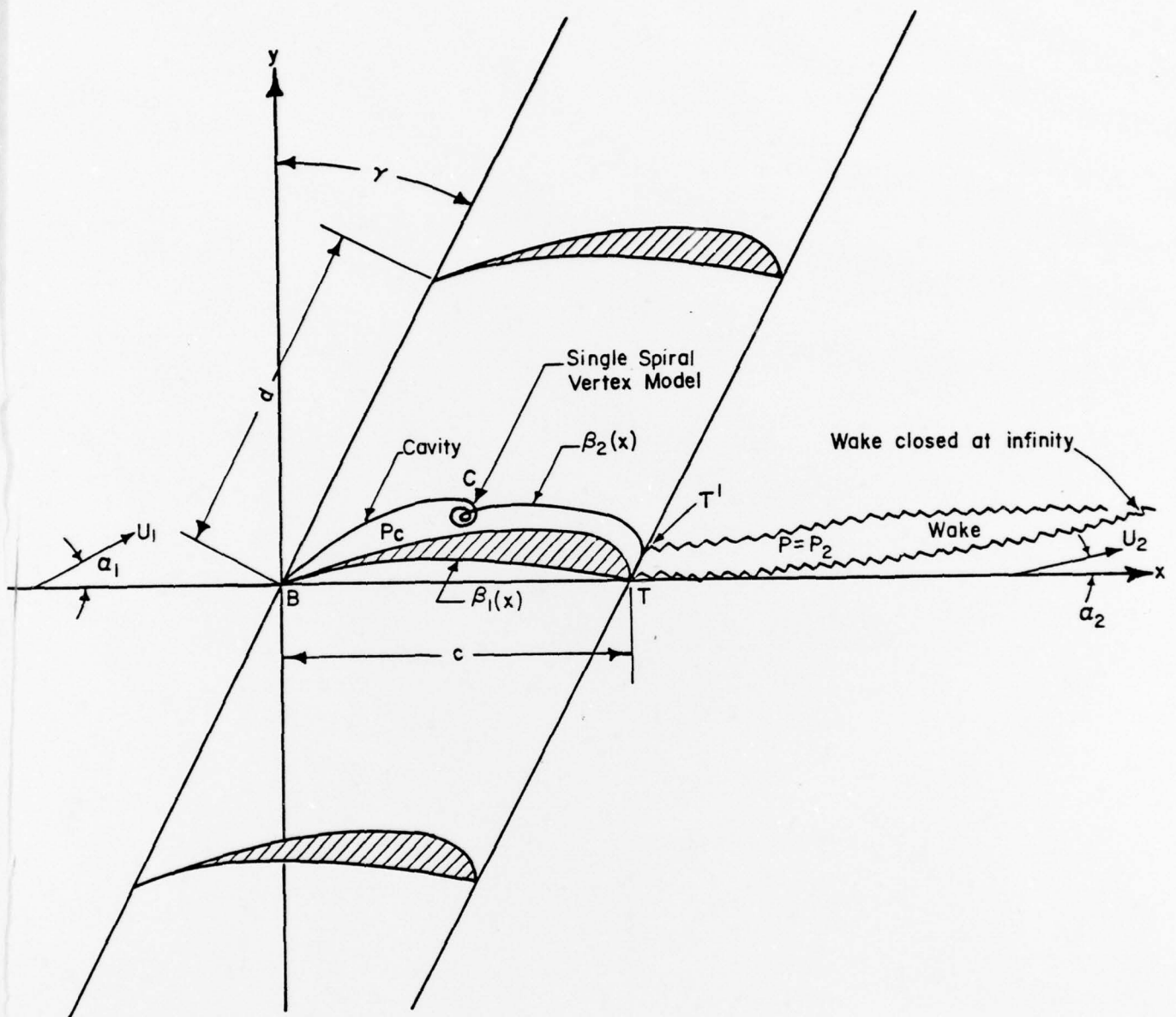
Figure 1   Flow configuration for partially cavitating cascade
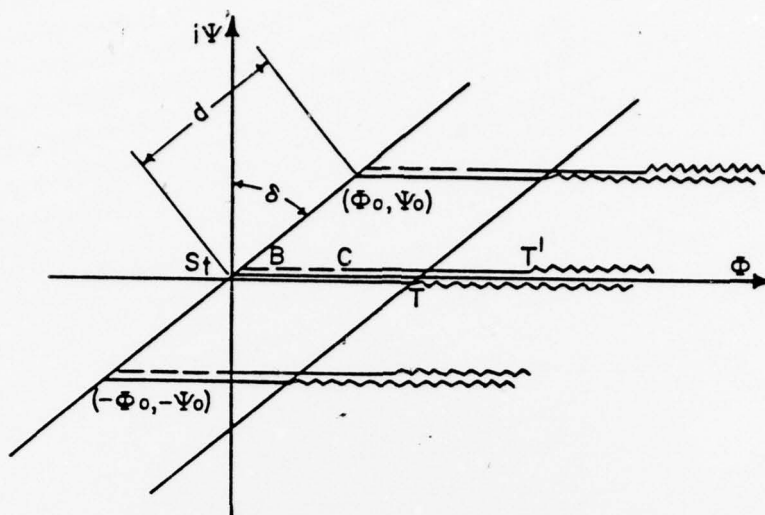
(a)   Potential plane $W = \Phi + i\Psi$
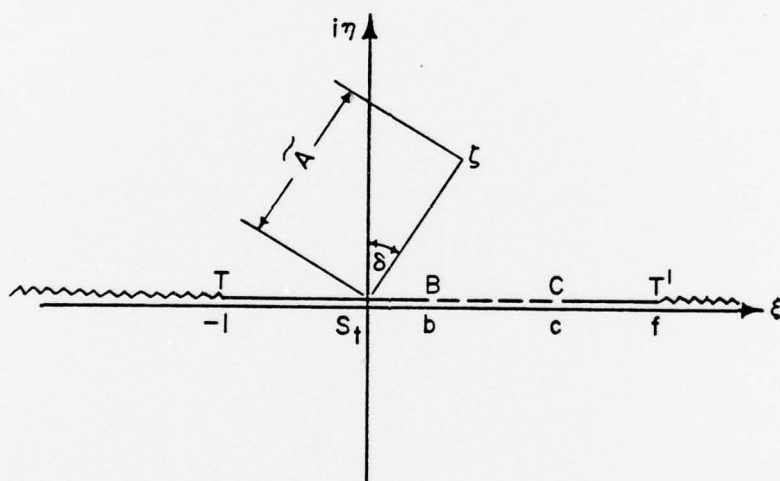
(b)   Transform plane $\zeta = \xi + i\eta$
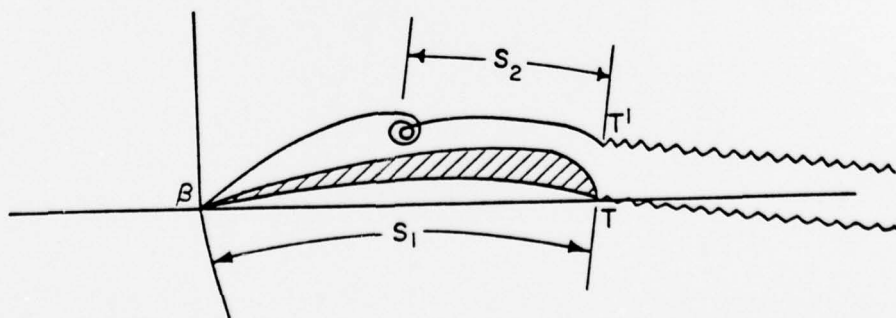
(c)   Definition of arc lengths S_1 and S_2.

Figure 2   Two transform planes and definition of arc
lengths S_1 and S_2.
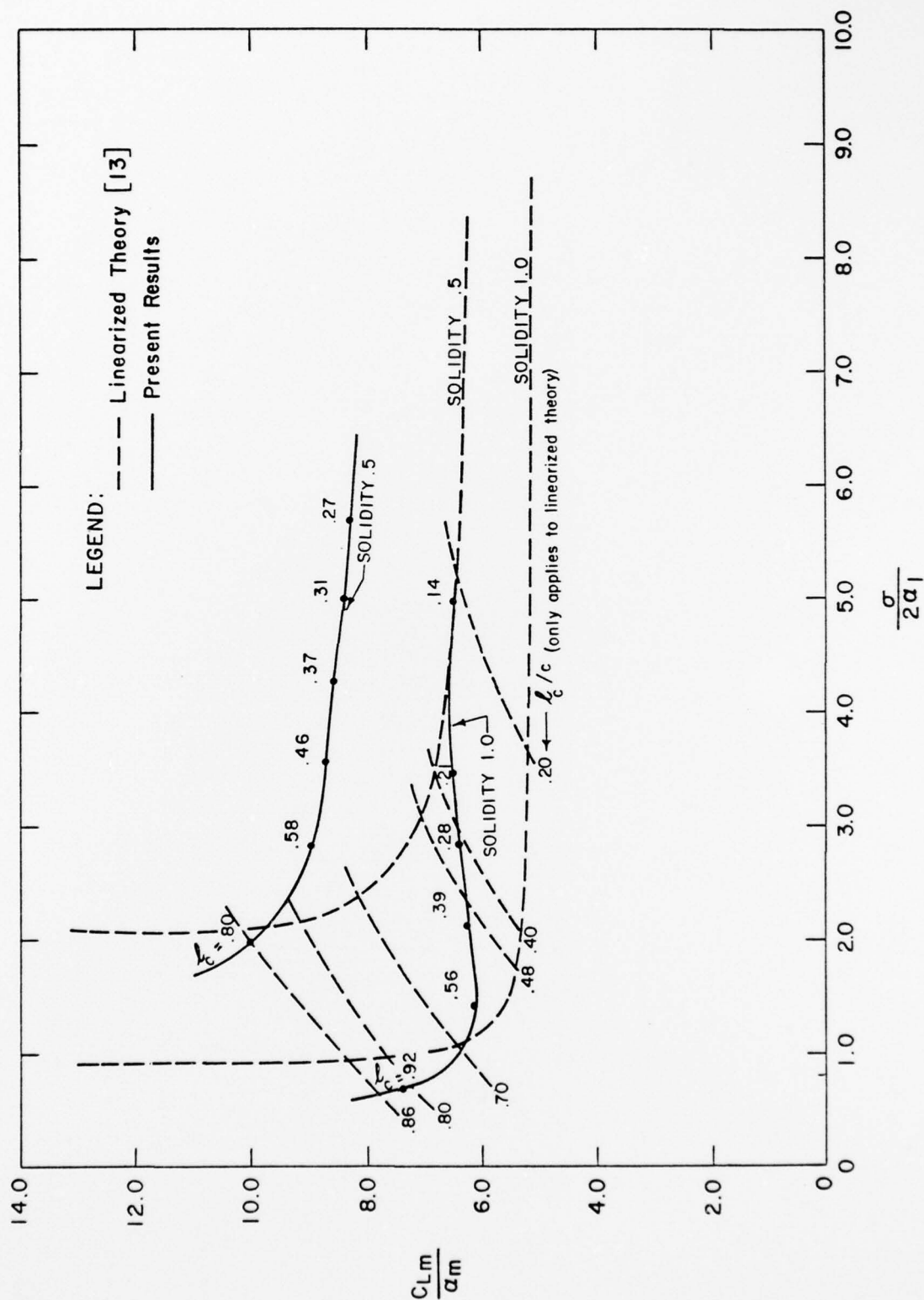
Figure 3   Comparison of the present theory with a linearized theory of Wade [13] for flat-plate cascade at $\alpha_1 = 8°$, $\gamma = 45°$ for two solidity cases, .5 and 1.0.
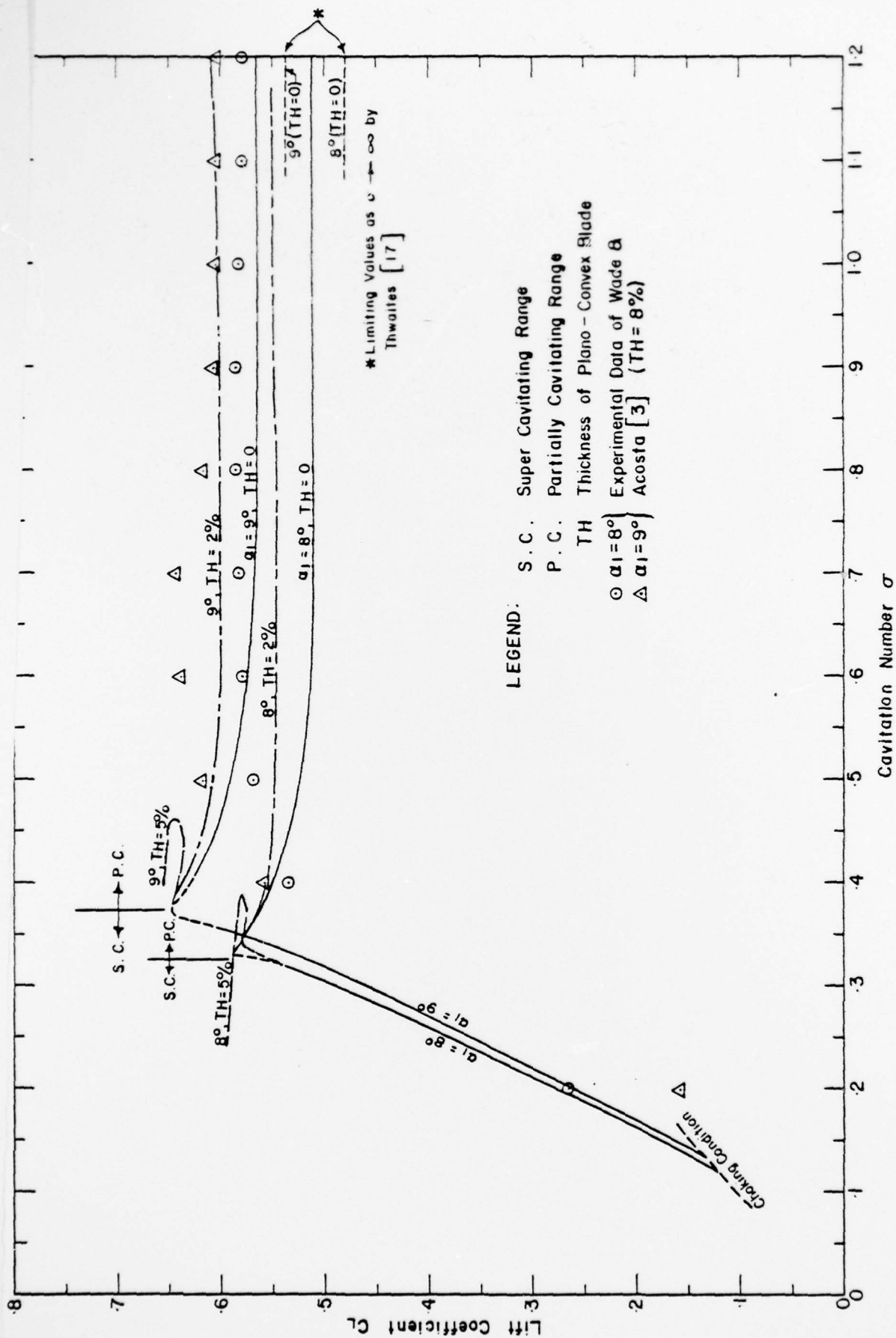
30

Figure 4   Comparison between the theory and experiment for plano-convex cascade having various blade thickness where solidity is .625 and stagger angles are 37° and 36° for $\alpha_1 = 8°$ and 9°, respectively (calculated data for supercavitating range made with [14] are also included).

31
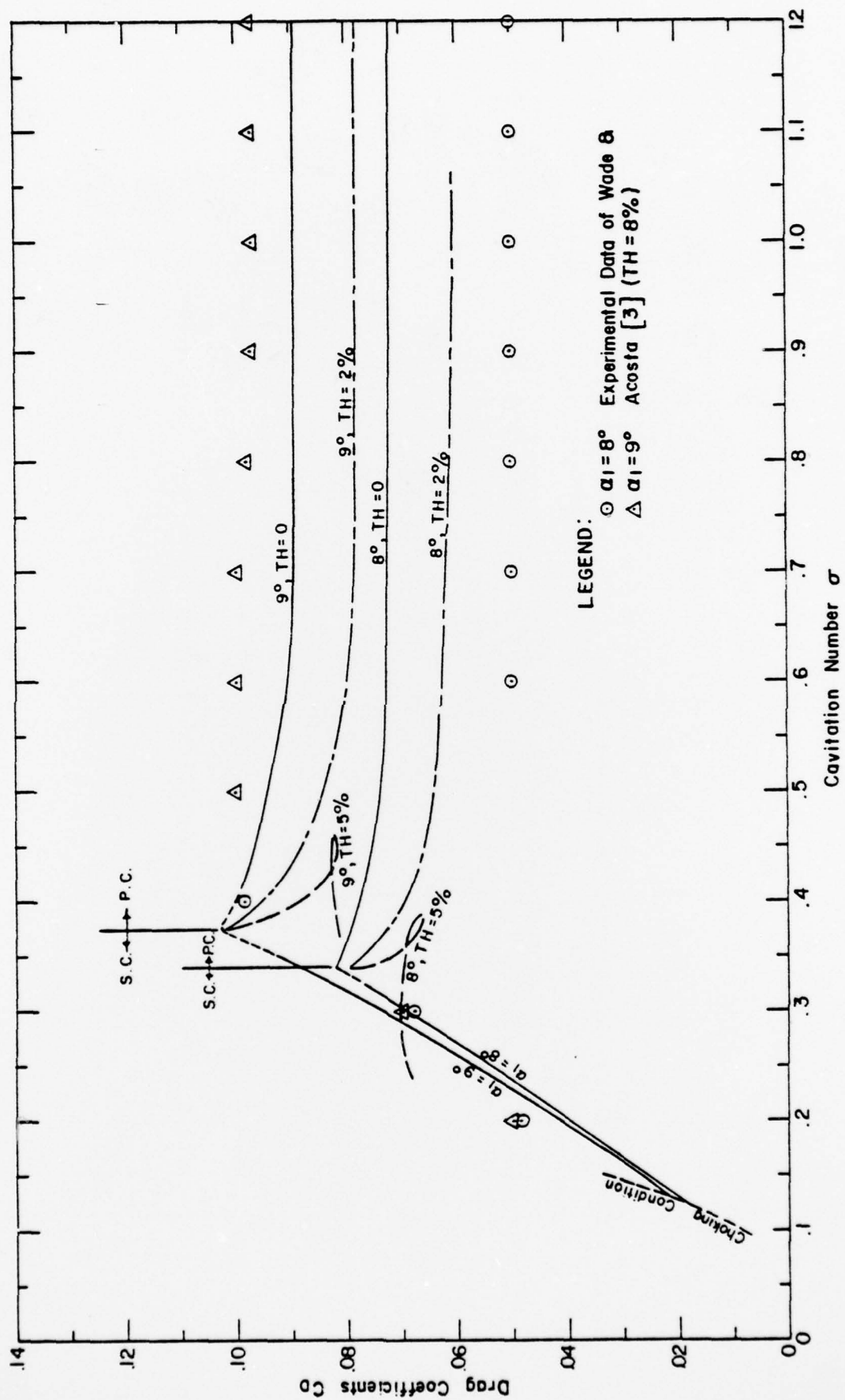
Figure 5   Drag coefficients for the same cases as Figure 4
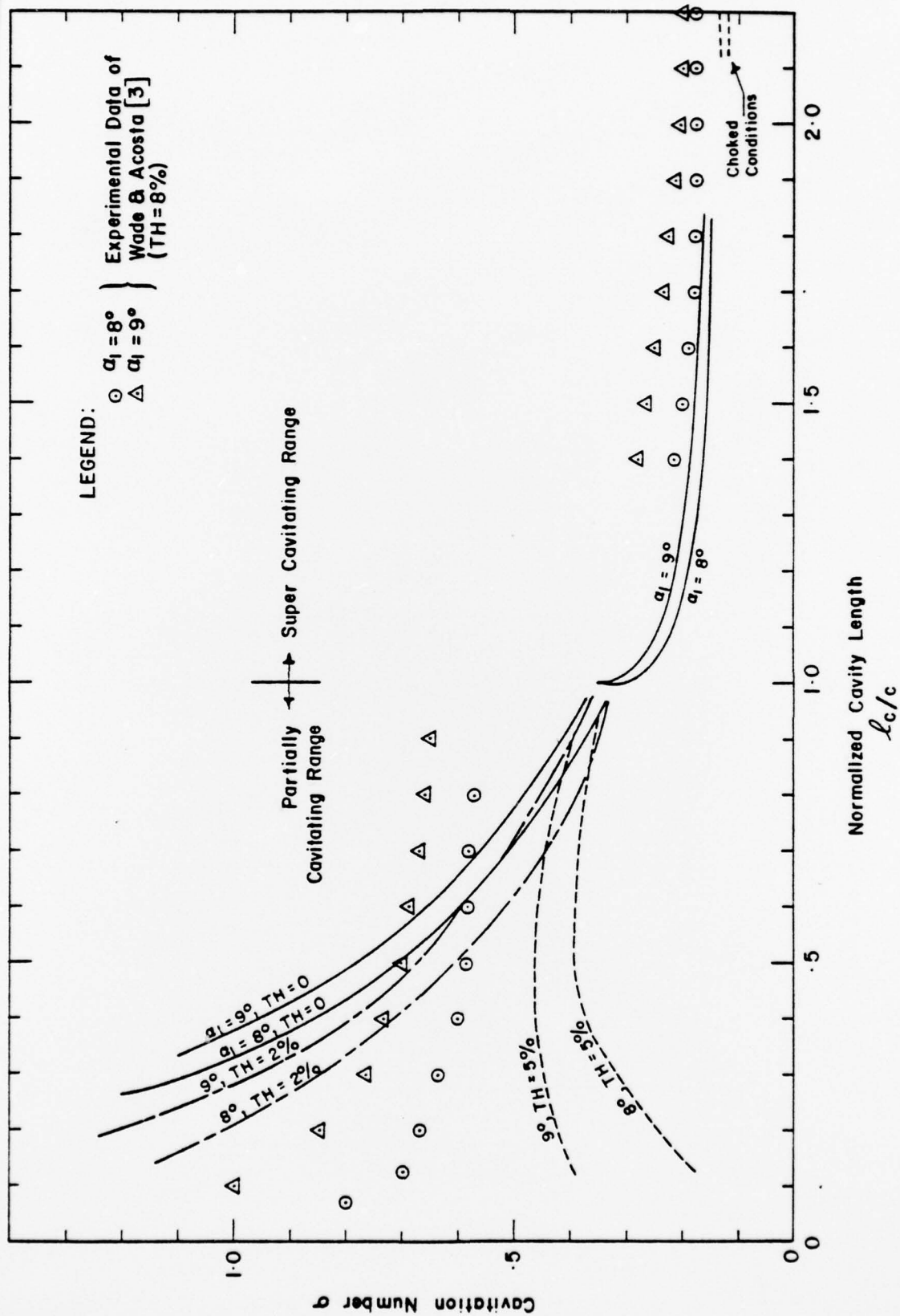
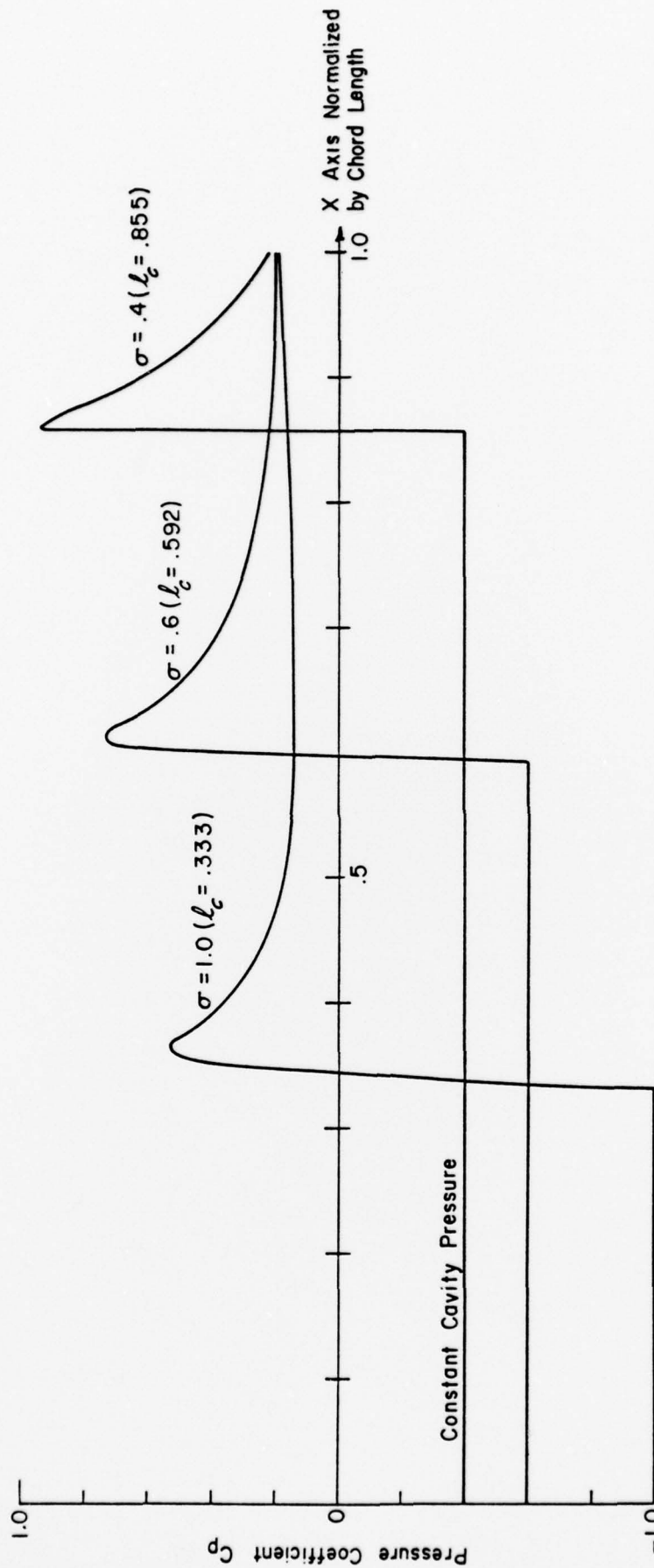Figure 6   Cavity length vs. cavitation number for the same cases as Figure 4.

Figure 7(a) Calculated pressure distribution on the upper wetted portion of plano-convex blade of partially cavitating cascade having 0 percent thickness for various cavitation numbers.
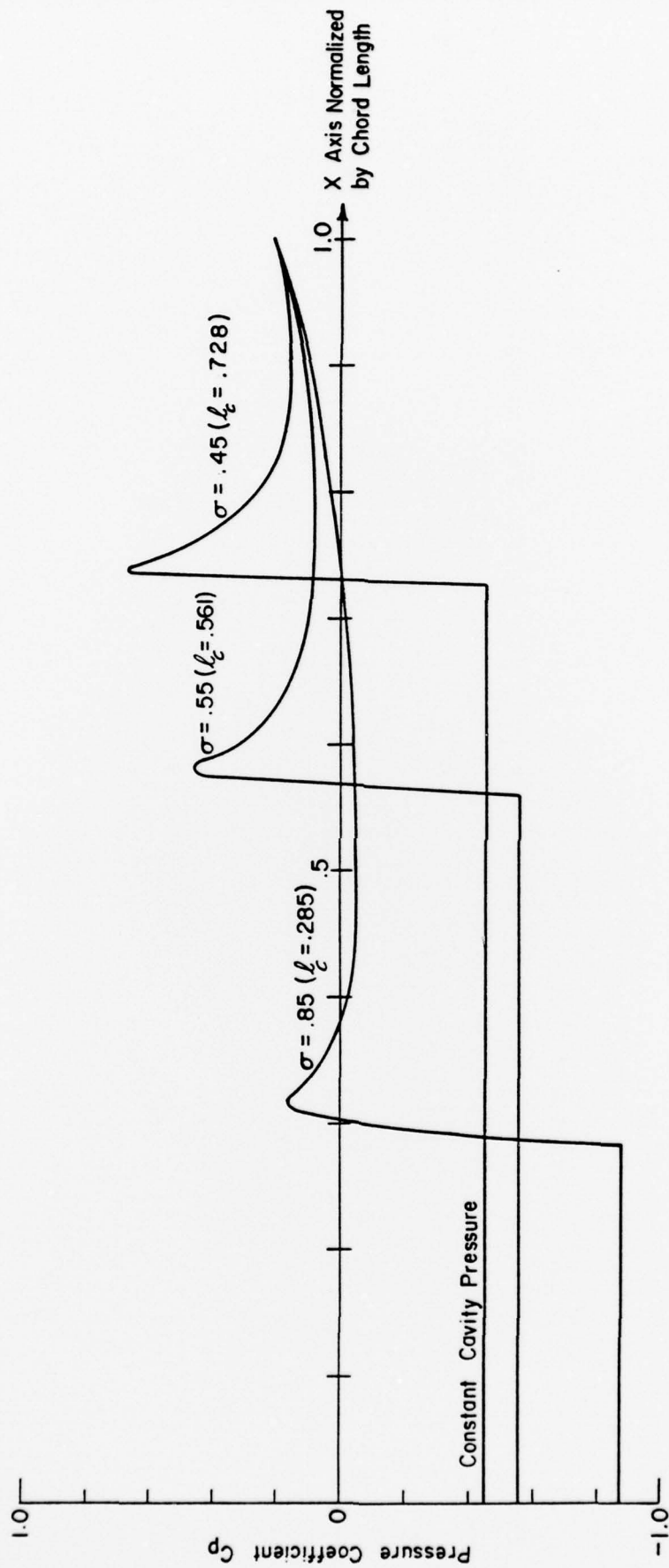
34

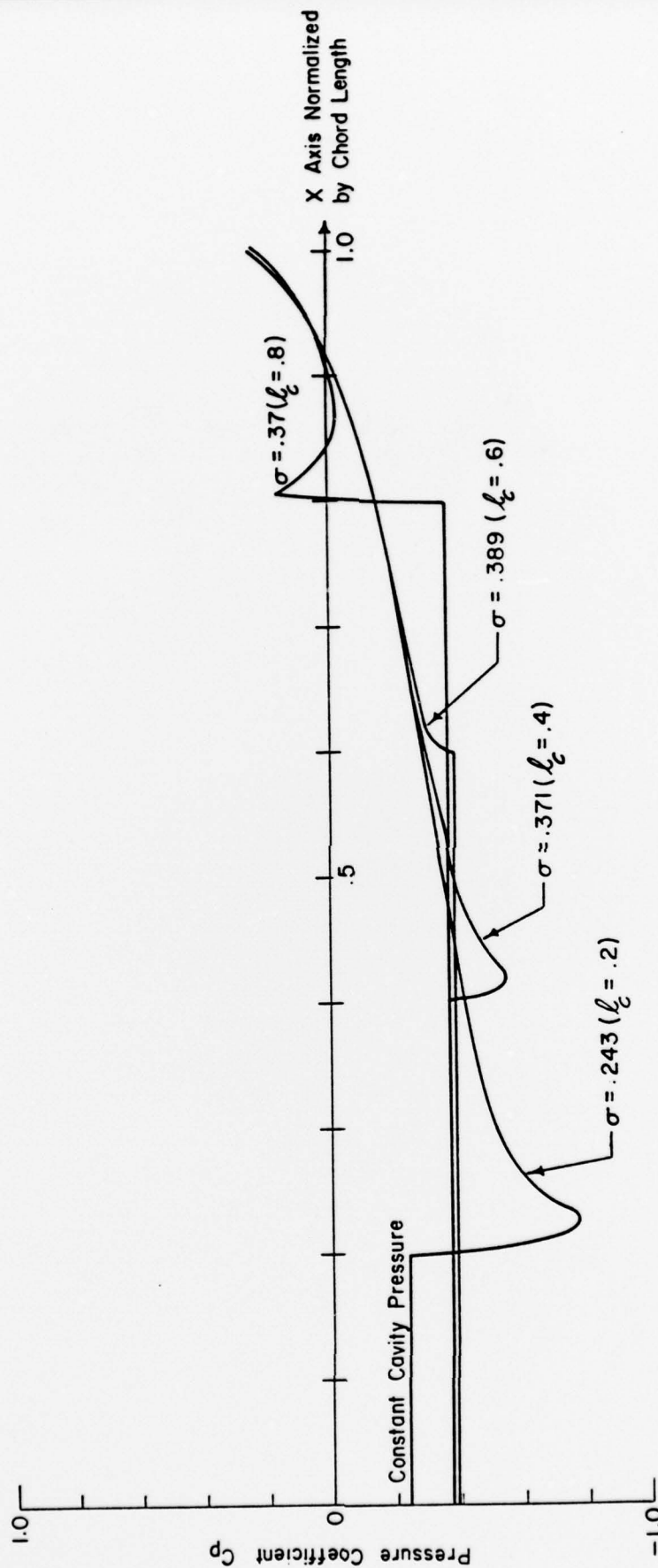Figure 7(b)   The same as Figure 7(a) except for TH = 2%.
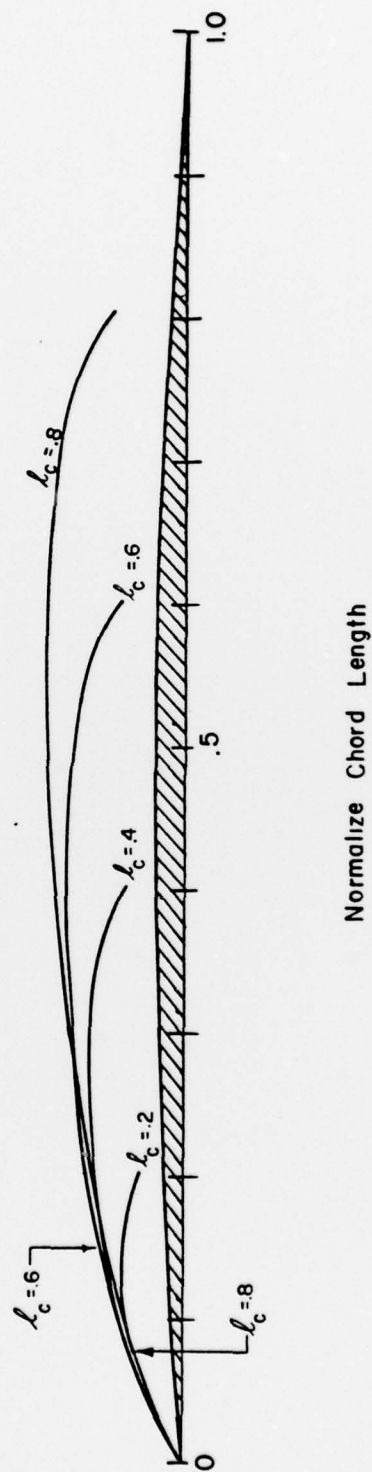
Figure 7(c) The same as Figure 7(a) except for TH = 5%.

36

Figure 8   Profiles of calculated cavity boundaries for cascade of plano-convex blades having 2% thickness at $\alpha_1 = 9°$ with $\gamma = 36°$ and solidity = .625